# Chitosan/montmorillonite nanocomposite film as anticancer drug carrier: A promising biomaterial to treat skin cancers

Ceramics International 50 (2024) 18528–18539

Contents lists available at ScienceDirect

Ceramics International

journal homepage: www.elsevier.com/locate/ceramint

# Chitosan/montmorillonite nanocomposite film as anticancer drug carrier: A promising biomaterial to treat skin cancers

Henrique Pereira Cardoso [a], José Filipe Bacalhau Rodrigues [a], Henrique Nunes da Silva [a], Taynah Pereira Galdino [a], Carlos Bruno Barreto Luna [a], Marcus Vinícius Lia Fook [a], Maziar Montazerian [a,b,**], Francesco Baino [c,*], Suedina Maria de Lima Silva [a,***]

[a] Academic Unit of Materials Engineering, Federal University of Campina Grande, Campina Grande, Paraíba, 58429-900, Brazil
[b] Department of Materials Science and Engineering, The Pennsylvania State University, University Park, PA, 16802, USA
[c] Institute of Materials Physics and Engineering, Department of Applied Science and Technology, Politecnico di Torino, Torino, 10129, Piemonte, Italy

ARTICLE INFO

*Keywords:*
Biomaterials
5-FU
Controlled release
Drug delivery system
Skin cancer

ABSTRACT

The solvent-evaporation approach was used to produce a chitosan (CS)/montmorillonite (MMT) nanocomposite film containing the anticancer drug 5-fluorouracil (5-FU). The physicochemical and morphological characteristics, drug release profile, cytotoxic and microbiological properties of the nanocomposite films were evaluated to verify their potential as a biomaterial for the treatment of tumors. X-ray diffraction (XRD) confirmed the formation of a CS-MMT/5-FU intercalated nanocomposite and Fourier transform infrared (FTIR) detected the characteristic 5- FU bonds in the CS/5-FU and CS-MMT/5-FU nanocomposite films, suggesting successful incorporation of the drug. The addition of 5-FU to chitosan increased the contact angle from 60.5° to 65.2°, which was compensated by the incorporation of MMT, resulting in a minimum contact angle of 42.7° (maximum hydrophilicity) for CS-MMT/5-FU. This result influenced the swelling degree and the *in vitro* release of 5-FU. The higher hydrophilicity of CS-MMT/5-FU promoted an increase in the swelling ratio compared to the CS/5-FU nanocomposite. CS-MMT/5-FU also showed a sustained, lower 5-FU release rate with antimicrobial activity against *S. aureus*, *E. coli* and *C. albicans* without inducing cytotoxicity or cell death. These results can be explained by the accommodation of the drug between the MMT lamellae, which maintains the 5-FU release without affecting its microbiological activity and reducing its toxicological effects. This work demonstrates that combining montmorillonite and chitosan in a nanocomposite film has the technological potential to control the release of 5-FU, resulting in a non-toxic antimicrobial drug carrier with promising potential for the treatment of skin malignancies.

## 1. Introduction

Both natural and synthetic polymers have been widely used to fabricate drug carriers. However, naturally occurring polymers have a helpful advantage over synthetic ones since they are less toxic, more biocompatible, biodegradable, easily available, and less expensive [1]. Among natural polymers, chitosan (CS) – a polycationic linear polymer obtained through the deacetylation of chitin and composed of D-glucosamine and N-acetyl glucosamine units joined by B-(1–4)-glycosidic bonds [2,3] – has gained enormous importance in biomaterials formulations and still is under intensive exploration in drug delivery systems. CS is a biopolymer with abundant sources, can undergo easy modification, is mucoadhesive, biodegradable, bioresorbable [4], innately biocompatible and non-toxic to living tissues [5], and exhibits antibacterial [5,6], antifungal [7], and antitumor activity [8,9]. CS can be used in various forms, including nano/micro-particles [10,11], gels [12], wires and meshes [13], scaffolds [14], and films [15] depending on the function and applications of the carrier. Nevertheless, some applications are limited because CS has low solubility in water, low colloidal stability, low mechanical strength, and a high expansion

*Abbreviations:* CS, Chitosan; MMT, Montmorillonite; 5-FU, 5-fluorouracil; XRD, X-ray diffraction; FTIR, Fourier transform infrared.

* Corresponding author.
** Corresponding author. Academic Unit of Materials Engineering, Federal University of Campina Grande, Campina Grande, Paraíba, 58429-900, Brazil.
*** Corresponding author.
*E-mail addresses:* mbm6420@psu.edu (M. Montazerian), francesco.baino@polito.it (F. Baino), suedina.maria@professor.ufcg.edu.br (S.M. de Lima Silva).

https://doi.org/10.1016/j.ceramint.2024.02.337
Received 11 August 2023; Received in revised form 30 January 2024; Accepted 26 February 2024
Available online 27 February 2024

rate [16]. To overcome these limitations, different types of CS nanocomposites have been studied as drug-delivery vehicles [17–19].

CS-clay nanocomposites have attracted increasing attention because of their structural and functional behavior. Montmorillonite clay (MMT), a soft phyllosilicate group of minerals with a 2:1 layered structure, is a naturally occurring aluminosilicate with an individual layer thickness of 1 nm, recognized by the Food and Drug Administration (FDA) as safe for food and medicine [20]. It is abundant, affordable, biocompatible, non-toxic, and stable under acidic conditions [21] and has been identified as one of the most suitable substances for the preparation of CS-based nanocomposites due to its large specific surface area, ion exchange capacity, adhesiveness, bioavailability, biodegradability, biocompatibility, and ability to release drugs in a controlled manner [19,22]. MMT increases the mechanical characteristics of CS and lowers its expansion after contact with aqueous solutions. In addition, the negatively charged surface of MMT may have strong electrostatic interactions with CS chains and enable the formation of functional nanocomposites. They show excellent mucoadhesive properties [23], high hydrolytic strength [24], interlayer nano-space formation [25] and, consequently, the ability to load different drugs in the interlamellar space [22,26].

Fluorouracil, also known as 5-FU, is a cancer antimetabolite medication that is frequently used in chemotherapy procedures [27]. When used as a cream, 5-FU is often provided alone or in combination with other anticancer medications to treat breast cancer, head and neck malignancies, anal cancer, stomach cancer, colon cancer, and several types of skin cancer [28]. Because 5-FU inhibits the operation of thymidylate synthase (TS) and erroneously incorporates its metabolites into RNA or DNA, it interferes with critical biosynthetic activity and produces cytotoxicity in tumor cells [27,29]. However, similar to other cancer treatments, its direct administration is associated with many side effects for patients [30]. This toxicity necessitates the development of drug delivery systems that allow the distribution of 5-FU in a targeted and safe way, with appropriate release capable of lowering systemic toxicity and limiting detrimental effects on healthy cells [31]. Hence, extensive efforts have been made to reduce these side effects and obtain highly efficient treatment via controlled drug releases.

Controlled release systems based on CS-MMT have been used to load and deliver 5-FU safely. When 5-FU was introduced into clay composites, CS-MMT nanocomposites showed slower drug delivery, reduced DNA damage, and hepatotoxicity, and no significant changes in 5-FU efficacy against tumor cells [32,33]. Studies have found that the strong binding of 5-FU with clay reduces toxicity and delays the profile of 5-FU release in CS-MMT composites [32,34–36]. Despite their controlled delivery capability, these systems exist primarily as powders [32], spheres [34], or films [35,36] intended for oral use. Other potential forms like film or gel [33,36] have been suggested but lack specific applications. Thus, the final form of these systems does not collaborate with a more versatile application. In addition, they do not fully cover treating other types of cancer, such as skin cancer delivery systems, which are currently non-existent. Table 1 presents a summary of the findings and limitations of CS/MMT nanocomposite systems loaded with 5-FU according to the current literature.

Given the scarcity of controlled release systems capable of treating a wide range of cancer types, we hypothesized that a nanocomposite in the form of a film based on CS-MMT loaded with 5-FU may prove to be a promising controlled release system capable of acting as an alternative for the treatment of skin cancer or other types of external cancer, given that CS-MMT clay nanocomposites have already been established as a promising drug carrier [19,22,37].

Although controlled release systems based on CS and MMT have been studied as carriers of 5-FU, nanocomposite films prepared with CS, MMT, and 5-FU for skin cancer treatment have not yet been investigated. In this study, CS-MMT nanocomposite films were prepared as a 5-FU carrier to be tested as a potentially promising biomaterial with low toxicity, antimicrobial activity and sustained 5-FU release to treat skin and other external tumors. The solvent evaporation approach was used to synthesize and characterize nanocomposite films. The physical, morphological, antimicrobial and biological properties of the nanocomposites were studied.

## 2. Materials and methods

### 2.1. Materials

5-FU in powder form (purity ≥99%) with a molar mass of 130.078 g/mol, polyoxyethylenesorbitan monooleate (Tween 80) and phosphate buffer saline (PBS) 0.1 M (pH = 7.2) were supplied by Sigma-Aldrich (code F6627-1G) (São Paulo, Brazil). Sodium MMT from Southern Clay Products (Texas, USA) was provided by Buntech (São Paulo,

**Table 1**
Selection of studies dealing with CS/MMT nanocomposite systems loaded with 5-FU.

| Material | Form | Application | Findings | Limitations | Ref. | Year |
|---|---|---|---|---|---|---|
| CS/MMT-rich bentonite/5-FU nanocomposite | Powder | Oral | The introduction of 5-FU into the nanocomposites resulted in a noteworthy postponement of DNA damage in lymphocytes. The nanocomposites maintained the anticancer efficacy of 5-FU while concurrently inducing a substantial decrease in hepatoxicity and pathological symptoms. | The nanocomposite's antimicrobial activity was not assessed. | [32] | 2012 |
| Alginate/CS/$Na^+$MMT/5-FU nanocomposite | Spheres | Oral | The nanocomposite showed a sustained release of 5-FU in pH ranges of 1.2, 7.4 and 10 suggesting the use of this nanocomposite for 5-FU release systems in the slightly basic environment of the small intestine. | The physical and biological properties of the nanocomposites, such as contact angle, degree of swelling, antimicrobial activity and cytotoxicity of the nanocomposite were not evaluated. | [34] | 2014 |
| CS/PVA/$Na^+$MMT/5-FU nanocomposite films | Film | Oral | Increased thermal stability, swelling ratio and load capacity with increasing MMT concentration. | The nanocomposite films presented low antimicrobial activity against *Salmonella* and *S. aureus* and no activity against *S. mutants* and *E. coli*; the cytotoxicity of the nanocomposite was not evaluated. | [35] | 2016 |
| CS/MMT/5-FU nanocomposite films | Film | Not proposed | Enhanced 5-FU loading capacity was achieved through the synergistic combination of CS and bentonite (commercially known as MMT), resulting in an extended 5-FU sustained release duration (>160 h) simulated under gastric fluid (pH 7.4) and intestinal fluid (pH 1.2) conditions. | No studies about the biological activity of composites (antimicrobial activity and cytotoxicity). | [36] | 2019 |
| Alginate/MMT/CS folate/5-FU gels | Gel | Not proposed | The composite exhibited heightened swelling capacity, sustained release capability for 5-FU, and cytotoxic activity against colorectal adenocarcinoma cells. | Lack of studies related to the morphology of the composite and its microbiological activity. | [33] | 2023 |

Brazil), which contained $Na^+$ ion as an interlayer cation, a density of 2.86 g/cm$^3$ and cation exchange capacity (CEC) of 92.6 meq/100 g, given by the supplier. CS used in this study was synthesized in the Northeastern Biomaterials Evaluation and Development Laboratory (CERTBIO, Campina Grande, Brazil) and had a molar mass of approximately 174 kDa and a degree of deacetylation (DD) of 82.9%. This CS is accredited by the National Institute of Metrology, Quality and Technology (INMETRO) at the International Organization of Standardization (ISO)/International Electrotechnical Commission (IEC) 17025:2005 and is used for medical applications. Maleic acid (C4H4O4, A.C.S. reagent, >99.9%) and sodium hydroxide (NaOH) were purchased from Neon Comercial (São Paulo, Brazil.). Hydrochloric acid (HCl, A.C.S. reagent, 37%) was provided by Quimica Moderna (São Paulo, Brazil). Distilled water was used to prepare all solutions.

### 2.2. Synthesis approach

Initially, an MMT/5-FU suspension was prepared. MMT was dispersed in distilled water (2 % w/v) and kept under magnetic stirring (200 rpm) for 30 min at room temperature (24 ± 2 °C). Then, the drug solution was obtained by solubilizing 10 mg of 5-FU in 20 mL of distilled water, with Tween 80 (0.5 % v/v) for 25 min, the necessary time for total solubilization of the drug. Next, the 5-FU solution was added to the MMT suspension. To avoid drug precipitation, the 5-FU solution was slowly added to the MMT suspension using an infusion pump model Pump 11 Elite (Harvard Apparatus, Holliston, USA). A 20 mL syringe was attached to the pump and the drug was added at a rate of 35 mL/h while the suspension was constantly stirred (200 rpm) using a magnetic stirrer. This method was employed since adding the drug too rapidly at room temperature can result in 5-FU precipitation [38]. After the addition of 5-FU in the MMT suspension the pH of the mixture was adjusted to 6 with 1 M HCl or NaOH solutions, depending on the nature of the mixture, to obtain protonated groups in the drug structure and possible interactions with the clay. The pH value was selected based on the pKa value of 5-FU which is 8.02, as verified in the literature [39]. Then, the resulting mixtures were kept under magnetic stirring (300 rpm) for 24 h, at room temperature (24 ± 2 °C), to be later added to the CS solution. The same procedure was followed to prepare the CS/5-FU film, but this time the 5-FU solution was prepared without its mixing with MMT suspension.

CS solution (2 % w/v) was prepared by dissolving CS powder in 50 mL of an aqueous maleic acid solution (2 % v/v). The maleic acid was selected due to the good physicochemical properties and noncytotoxic of the films compared to those obtained with other acids (acetic acid, lactic acid, tartaric acid and citric acid) [15]. CS solution was continuously stirred under 500 rpm for 2 h at room temperature (24 ± 2 °C) to obtain a homogeneous mixture. In the preparation of the CS nanocomposites with 1 wt% of 5-FU and 1.5, 3.0 and 5.0 wt% of MMT (CS-1.5MMT/5-FU, CS-3.0MMT/5-FU, CS-5.0MMT/5-FU), the MMT/5-FU suspensions prepared previously were slowly added to the CS solution and then the new suspension was stirred (500 rpm) for other 2 h at room temperature (24 ± 2 °C). Subsequently, the suspension was filtered with the 100 μm filter to separate possible insoluble particles and impurities. Then, the suspension was poured into 10 × 10 cm$^2$ Teflon Petri dishes, where it remained at rest for 24 h at room temperature (24 ± 2 °C) until the air bubbles were eliminated. The plates were taken to an oven at 37 °C for 72 h for complete solvent evaporation and film formation (thickness of ~150 μm). The pure CS films and the CS films containing 1 wt% 5-FU (CS/5-FU) were also prepared in the same way. As the pH of the films (pH = 6) is similar to that of the skin (between 4.1 and 5.8) [40] and since the 5-FU was fully solubilized in the solvent, washing was not necessary for neutralization or to remove any unbound drug. In addition, considering that the 5-FU was fully solubilized in the solvent, it can be assumed that 100% of the 5-FU is present and attached to the films. Before characterizations, the dried films were stored in a controlled temperature and humid environment (25 °C and relative humidity of 40–60%).

### 2.3. Characterization methods

#### 2.3.1. X-ray diffraction (XRD)

XRD analyses were conducted to evaluate the crystallinity of CS, MMT, and 5-FU, as well as to investigate the incorporation of 5-FU between MMT layers and assess the crystallinity of the nanocomposite films. The analysis was carried out in an XRD-7000 Shimadzu diffractometer (Shimadzu, Kyoto, Japan), using copper Kα radiation (1.5418 Å), a voltage of 40 kV, current of 30 mA, speed of 1°/min, step size of 0.02° and in a 2–40° range. The calculation of the interplanar distance $d_{001}$ was carried out according to Bragg's equation.

#### 2.3.2. Scanning electron microscopy (SEM)

SEM was used to evaluate the surface morphology of the nanocomposite films using a Pro-X800-07334 microscope (Phenom-World, Eindhoven, The Netherlands), at magnifications of 500 × and 2000 × using 15 kV voltage, with a depth of focus of 1 mm and a resolution of 30 nm. The samples were placed on double-sided carbon tape and were coated with a thin layer of gold.

#### 2.3.3. Fourier transform infrared spectroscopy (FTIR)

FTIR analyses were conducted to assess interactions between chitosan, clay and drug. FTIR was performed on a Perkin Elmer 400 FT Mid-IR, (Perkin Elmer, Waltham, USA) equipped with attenuated total reflectance (ATR) accessory equipped with zinc selenium (ZnSe) crystal, scanning from 4000 to 650 cm$^{-1}$, with a resolution of 4 cm$^{-1}$ at room temperature (24 ± 2 °C) and 32 scans.

#### 2.3.4. Swelling degree

Swelling degree analyses were performed to determine the absorption capacity of the nanocomposite films in PBS. The swelling analysis was performed according to a procedure reported in the literature [35]. The films were prepared with a surface area of 1 cm$^2$, dried in an air-circulated oven for 24 h at 37 ± 0.5 °C (average human body temperature) and weighed on an analytical balance. Then, the films were immersed in a glass beaker containing 5 mL of phosphate buffer solution (PBS; pH = 7.2). The swelling degree of the films was measured at time intervals of 0, 1, 3, 6 and 24 h. The swelling degree (SD%) of the films was calculated using Equation (1):

$$SD\ (\%) = W_d\text{-}W_s/W_s \quad (1)$$

Where Wd is the weight of the swollen film at different time intervals and Ws is the weight of the dry film. The assay was performed in triplicate and the results were analyzed as an average of three samples.

#### 2.3.5. Water contact angle

The water contact angle (θ) was used to measure the wettability of the nanocomposite films. The analyses were carried out by the sessile drop method, using a portable contact angle measurement unit model Phoenix-i from (Surface Electro Optics, Suwon, South Korea). A water drop was put on the film surface using a micrometer doser, and the image was captured and analyzed by the Phoenix-i.

#### 2.3.6. In vitro drug release studies

To determine the release profile of nanocomposite films the amount of 5-FU released from CS and CS/MMT films was measured using an ultraviolet–visible (UV-VIS) spectrophotometer model 1800 (Shimadzu, Kyoto, Japan). First, the films (with a mass-to-solution ratio of 25 μg mL$^{-1}$) were incubated in a volumetric flask in an 800 mL PBS solution (pH = 7.2) that was selected as a release medium since this is used in biochemistry to mimic human extra-cellular fluid [41]. Next, the volumetric flasks were kept under constant stirring of 50 rpm in a shaker model KS4000i (IKA Werke, Staufen, Germany) at 37 °C ± 0.5 °C to

simulate body temperature. Subsequently, an aliquot of the PBS (3 mL) was taken at fixed time intervals (1 h, 1h 30 min, 2 h, 2 h 30 min, 3 h, 3 h 30 min, 4 h, 4 h 30 min, 5 h, 20 h and 24 h), and replaced with 3 mL of a fresh PBS (at 37 °C ± 0.5 °C) each time. The samples were then analyzed for 5-FU content by measuring the absorbance at 266 nm ($\lambda_{max}$ of 5-FU in PBS, pH 7.2, measured using a UV-VIS spectrophotometer). All the release experiments were carried out in triplicate, and the average values were used for further data treatment and plotting. The drug concentration was calculated according to a standard curve and Equation (2) to determine the cumulative release. The corresponding drug-release profiles were represented through plots of the cumulative percentage of drug release (calculated from the total amount of 5-FU contained in each sample) versus time.

$$\text{Cumulative release } (\%) = \frac{\text{Amount of 5-FU in PBS solution}}{\text{Amount of 5-FU added to the films}} \times 100 \quad (2)$$

#### 2.3.7. Antimicrobial activity

The antimicrobial properties of the 5-FU solution and CS/5-FU and CS-5.0MMT/5-FU films were evaluated by the disk-diffusion method. Strains of *Staphylococcus aureus* (ATCC 13656), *Escherichia coli* (ATCC 25422), and *Candida albicans* (ATCC 76645), commonly found in external wounds, were selected for the assay.

Initially, bacterial and fungal suspensions were prepared at concentrations of 0.5 on the McFarlad scale, using a 0.005 M PBS solution. Then, with the aid of a swab, the suspensions were spread on Milan Hinton Agar (MHB) plates. The 5-FU solution at 125 μg $mL^{-1}$ (concentration present in the films) was added to sterile filter paper and applied to the MHB plates with the microbial inoculum, while samples of the nanocomposite films were applied to the plates in the form of 5 mm diameter discs. The plates were incubated inverted in a bacteriological incubator at 35 °C for 48 h. The results were reported as the average of the two inhibition zones measured (24 and 48 h) without subtracting the disc diameter.

For the assay, MHB culture media were used, supplemented with solidifying medium (Bacto Agar). Vancomycin was used as a positive control for bacterial strains, and saline solutions were used as negative controls for all microorganisms. A positive control was not used for the fungal strain. All strains used had 24 h growth. The analysis was conducted in triplicate.

#### 2.3.8. Cytotoxicity - agar diffusion assay

The agar diffusion assay was performed according to ISO 10993-5 2009 standard to evaluate the cytotoxicity of films. A mouse fibroblast cell line L929 (ATCC NCTC clone 929, Banco de Células do Rio de Janeiro, Brazil) was used since this cell type is recognized as a reference for cytotoxicity tests of biomaterials that are intended for contact/treatment of lesions present in the skin [42]. The L929 cells were cultured in RPMI 1640 medium Gibco® (Invitrogen Corporation, Waltham, USA) and incubated in a humidified oven at 37 °C and with 5% $CO_2$ until reaching 80% confluence. Then, trypsinization with 0.25% trypsin Gibco® (Life Technologies, Carlsbad, USA) and cell counting was performed using an automatic cell counter from Interwoven (Thermo Fisher, Waltham, USA). Suspensions of $1.0 \times 10^5$ cells/mL were distributed in 6-well plates, with 4 mL added to each well, lasting 24 h. Upon verifying the uniform confluence of 80% on the plates, with the aid of a microscope, the culture medium was suctioned and 1 mL/well of medium prepared with 2 × concentrated MEM Gibco® (Invitrogen Corporation, Waltham, USA) was added to 1.8% agar solution with 0.01% neutral red (Sigma-Aldrich, USA), which remained protected from light at room temperature (24 ± 2 °C) for 10 min for solidification. The samples were evaluated according to the standard, using a concentration of 200 mg/mL as an extract in PBS, incubated at 37 °C for 24 h. The incubation period was selected according to the time used in drug release studies in order to test the samples during the period with the greatest release of 5-FU. Thus, with this conditions it is possible to assure a sufficiently prolonged exposure time of the cells to the extracts and, furthermore, a critical exposure condition given the high concentration of the extracts.

To evaluate the sample, filter paper sectioned in 1 $cm^2$ was inserted in the center of each well in duplicate. Growth control (healthy cells), Positive (toxic latex), and negative (quantitative filter paper) controls were inserted in duplicate. The plates were wrapped in aluminum foil and incubated in an inverted position for 24 h in a humidified oven at 37 °C and 5% $CO_2$. Following the standard guideline, the bleaching zones around the sample were measured. An inverted microscope model Eclipse TS100 (Nikon, Tokyo, Japan) was used to analyze the cell lysis, which was classified according to Table 2.

## 3. Results and discussion

### 3.1. Morphological characterizations

Fig. 1 shows the XRD patterns and SEM images of 5-FU, MMT, as well as CS, CS/5-FU, CS-1.5MMT/5-FU, CS-3.0MMT/5-FU and CS-5.0MMT/5-FU nanocomposite films. This figure also shows possible interactions between CS, 5-FU, and MMT and some data about the basal spacing degree of the MMT.

The diffractogram of 5-FU showed an intense peak at 2θ = 28.9° (Fig. 1A), suggesting its crystalline structure [34,43,44]. Moreover, some peaks with lower intensity are observed at 2θ = 16.5, 19.3, 20.7, 22.1, 31.5, 32.2 and 33.5°, in accordance with the literature [34,44,45]. The MMT diffractogram (Fig. 1A) showed a peak around 2θ = 6.06°, corresponding to a basal interplanar distance ($d_{001}$) of 1.46 nm, which is characteristic of sodium MMT with one $H_2O$ molecule layer inside the interlaminar space [35,46,47]. The other peaks at 19.9° and 28.8° indicate the turbostratic stacking of layers [48].

XRD patterns of the CS film (Fig. 1A) showed two small peaks at 2θ = 10.98° (020 plane) and at 17.52° (100 plane) combined with a broad diffraction centered at around 21.03° (110 planes). The former two peaks indicated the crystalline structure of the hydrated chitosan polymorph, whereas the broad peak around 21.03° indicated the existence of an amorphous structure [49]. This is in good agreement with the diffraction pattern of CS reported by other authors [49–52], which proves a semicrystalline nature of CS film with form I crystals [53]. Compared to pure CS film, the CS/5-FU film exhibits a higher crystallinity or denser packing, as indicated by sharper peaks with higher intensity. In addition, a small peak was observed at around 15.86° in CS/5-FU film, which has been attributed to the crystal lattice of the anhydrous chitosan polymorph [54]. Another important observation relative to the CS/5-FU film diffractogram is that the characteristic peaks of 5-FU are not seen. This finding is in line with the results obtained by Li, Wang, Peng, She and Kong [45] and may be explained by the fact that the 5-FU drug interacts with CS at the molecular level (Fig. 1D) and is observed existing in an amorphous state in the CS. For this reason, SEM images of CS/5-FU film (Fig. 1B) show an homogeneous and smooth surface without any apparent phase separation like in the pure CS film.

The XRD patterns of CS-clay/drug nanocomposite films with total filler contents of 1.5, 3.0, and 5.0 wt% and 1 wt% drug (CS-1.5MMT/5-FU, CS-3.0MMT/5-FU, and CS-5.0MMT/5-FU) are also shown in Fig. 1A. The addition of 1.5 wt% MMT to the CS/5-FU film resulted in a

**Table 2**
ISO-10993-5 criteria for agar diffusion assay reactivity score.

| Grade | Reactivity | Description of the reactivity zone |
|---|---|---|
| 0 | None | No detectable zone around or below specimen |
| 1 | Light | Some malformed or degenerated cells under specimen |
| 2 | Soft | Zone limited to the area under specimen smaller than 0.45 cm |
| 3 | Moderate | Zone extension sample size up to 1.0 cm |
| 4 | Severe | Zone that extends beyond 1.0 cm beyond the sample |

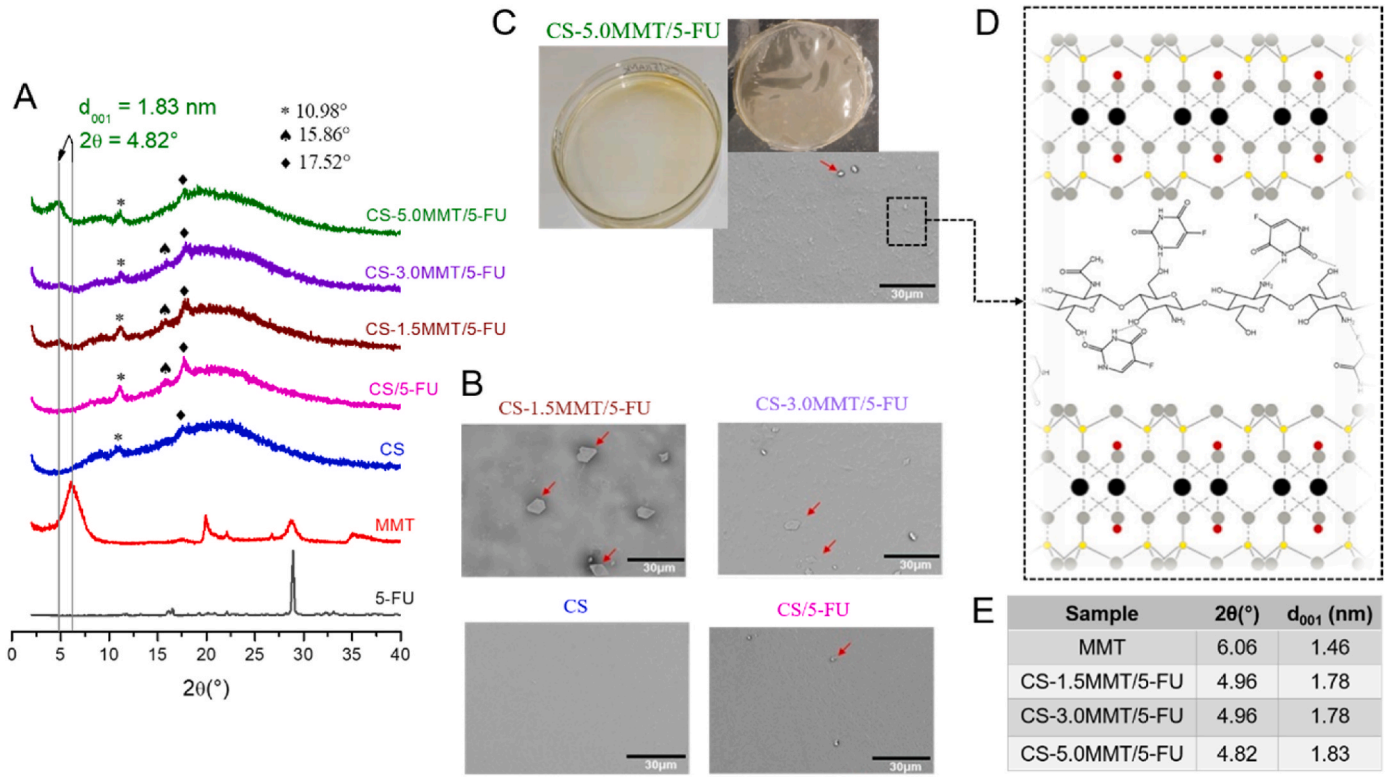


**Fig. 1.** (A) XRD patterns; (B) SEM images; (C) images of the nanocomposite films; (D) illustration of the proposed interactions among CS, 5-FU, and MMT, and the formation of the intercalated structure nanocomposite; and (E) the XRD pattern of MMT clay and the basal spacing ($d_{001}$) data calculated using Bragg's equation for the nanocomposite films. The red arrows indicate the presence of agglomerates. (For interpretation of the references to color in this figure legend, the reader is referred to the Web version of this article.)

reduction in the intensity of the peak at 15.86°, which corresponds to the crystal lattice of the anhydrous chitosan polymorph. The same effect was observed for films with higher MMT content (CS-3.0MMT/5-FU and CS-5.0MMT/5-FU), which, in addition to the reduction in the intensity of the 15.86° peak, also showed a decrease in the intensities of other XRD peaks, especially for the CS-5.0MMT/5-FU nanocomposite film, where the peak around 15.86° was not detected. This reduction in peak intensity suggests that the addition of MMT results in a more amorphous film due to the water molecules present between the clay layers, which favor the reduction of the anhydrous chitosan polymorph.

The presence of CS and 5-FU chains facilitated the opening of the clay lamellae in all CS-clay/drug films (Fig. 1E), resulting in a shift of the XRD peak of MMT clay from 6.06° to a maximum of 4.82°, corresponding to a basal spacing ($d_{001}$) of 1.46 nm and 1.83 nm, respectively. Because the thickness of the individual sheet of the CS chain is 0.38 nm [50], these results imply CS intercalation with MMT as a monolayer, as shown in Fig. 1D. Also, the increase in basal spacing indicates the formation of a "sandwich model of CS/5-FU/CS" (Fig. 1D) inside the gallery of the MMT since this structure enhances the electrostatic interactions between 5-FU, CS and clay layers [32,33]. This proves the successful loading of CS and 5-FU molecules between the MMT layer, resulting in an intercalated structure nanocomposite with increased clay basal spacing but maintained multilayer stacking. These findings are in agreement with Bragg's law which mentions that a shift in 2θ value from a higher diffraction angle to a lower diffraction angle is indicative of an increase in *d*-spacing [33,35] and are consistent with earlier publications [33–35,46,55–57].

Although the formation of nanocomposites was observed for all compositions, the amount of MMT clay utilized in the film preparation altered MMT dispersion in the matrix, as revealed by SEM images in Fig. 1B. Some aggregates were found for CS-1.5MMT/5-FU and CS-3.0MMT/5-FU nanocomposites, as indicated by red arrows in Fig. 1B. However, for CS-5.0MMT/5-FU nanocomposite, MMT clay showed a homogeneous distribution in CS matrix (Fig. 1C), which may be attributed to 5-FU and CS entering and sitting between clay layers and to the polycationic ability of the CS that attracted the MMT forming a physical bond between them as described by Reddy et al. [35]. These findings are consistent with XRD data, which showed lower crystallinity or denser packing for the CS-5.0MMT/5-FU nanocomposite, indicating a more amorphous film caused by a decrease in interactions among CS macromolecules while maintaining layered stacking, primarily with alternating layers of CS and MMT. Thus, it was possible to confirm the dispersion of MMT in the nanocomposite films, identify the presence of clay in the chitosan films, as well as the presence of 5-FU between the MMT lamellae.

### 3.2. Chemical characterization of nanocomposite films

Fig. 2 displays the FTIR spectra of 5-FU, MMT, as well as CS, CS/5-FU and CS-clay/drug nanocomposite films. The vibration bands at 3125–2829 $cm^{-1}$ in the 5-FU spectrum were attributed to aromatic and aliphatic C–H stretching vibrations. The band at 1650 $cm^{-1}$ suggested stretching vibrations of the tertiary amide and 1502 $cm^{-1}$ the bending vibration of the N–H group. C–N stretching vibration and flexural vibration in the C–H plane of the CF–CH group were indicated at 1248 $cm^{-1}$ and 1430 $cm^{-1}$, respectively. In addition, the bands at 804 $cm^{-1}$ and 751 $cm^{-1}$ were related to out-of-plane C–H vibration of the CF–CH group [32].

In MMT, the bands within 3630–3500 $cm^{-1}$ were attributed to the vibrations of hydroxyl structural stretching (O–H) between the clay layers. The peak at 1640 $cm^{-1}$ suggested the bending vibration of the H–O–H bonds present in the water molecules adsorbed onto the MMT surface [58]. Stretching vibrations of Si–O–Si bonds were observed in the range of 1050 to 1030 $cm^{-1}$ [59].

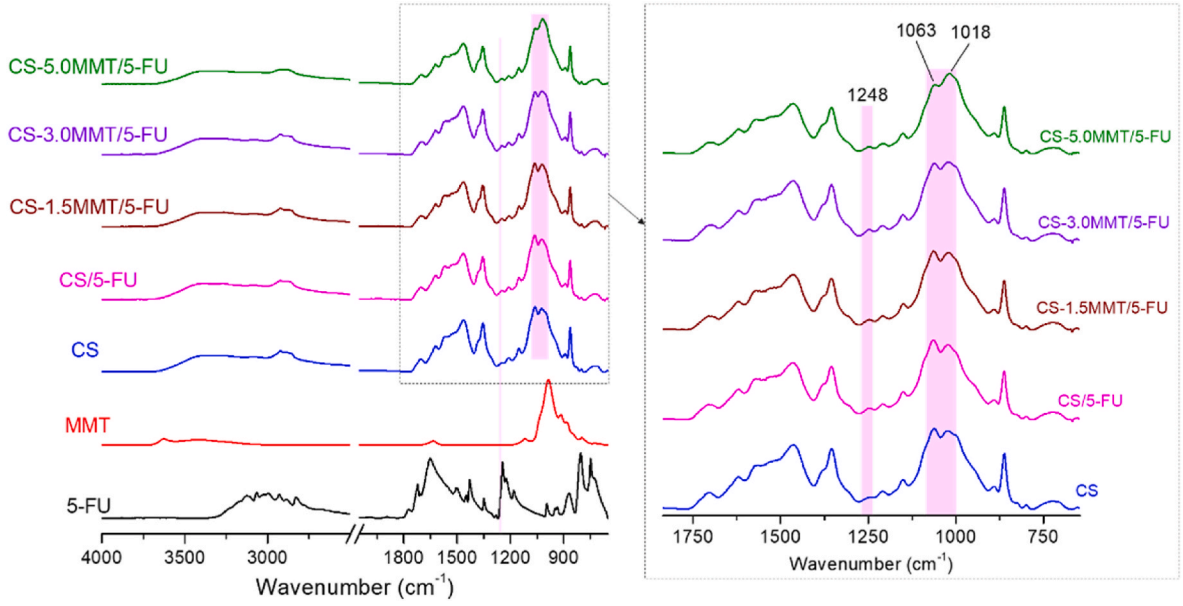


**Fig. 2.** FTIR spectra of pure materials (5-FU and MMT) and CS, CS/5-FU and CS-5.0MMT/5-FU films.

The FTIR spectrum of the CS showed peaks between 3450 and 3022 $cm^{-1}$, suggesting axial deformation of the O–H and N–H groups [60]. The bands at 2923 $cm^{-1}$ and 2880 $cm^{-1}$ were associated with the stretching vibration mode of the –CH $sp^3$ carbon bond [61], respectively. The spectrum also showed an intense peak at 1702 $cm^{-1}$, referring to the axial deformation of C]O of amide I [62]. The vibrations of the amine group ($–NH_2$) and the vibrational deformation of the protonated amine group ($–NH_3^+$) could be verified with the bands at 1620 $cm^{-1}$ and 1568 $cm^{-1}$, respectively. In addition, the band at 1464 $cm^{-1}$ was typical of the angular deformation of C–H ($–CH_2$ and $–CH_3$) [63]. The intense absorption bands in the 1151 $cm^{-1}$ and 892 $cm^{-1}$ range indicated the presence of glycosidic bonds (C–O–C). At the same time, bands around 1063 $cm^{-1}$ and 1018 $cm^{-1}$ were elongation vibrations of the C–OH group in the CS chain [64,65].

After introducing 5-FU, the CS spectrum revealed a new peak at 1248 $cm^{-1}$ (CS-clay/drug films spectrums in Fig. 2), confirming the interactions between 5-FU and CS. Other vibration bands characteristic of 5-FU were not observed due to the drug's intercalation into the silicate layers of MMT, which resulted in less interaction between 5-FU and CS [34]. The CS-5.0MMT/5-FU nanocomposite film spectrum showed a change of the band at 1063 $cm^{-1}$ intensity in relation to 1018 $cm^{-1}$ (Fig. 2). The change in intensity is related to the overlapping of vibrations of the secondary amide and Si–OR groups and indicates interactions between CS and the MMT phase [36]. This observation demonstrates conclusively that either 5-FU or MMT interacted with CS, which is in good agreement with XRD results and another report [32, 34].

After the presence of 5-FU and MMT in the CS-clay/drug films was detected, a contact angle analysis was conducted. The contact angle measurement allows for checking the hydrophilicity or hydrophobicity of the materials. The behavior is related to surface tensions and interactions, i.e. the wetting capacity. Three classifications exist according to the contact angle, namely hydrophilic ($\theta < 90°$), hydrophobic ($90° < \theta < 150°$), or totally hydrophobic ($\theta > 150°$) surface [15]. Fig. 3 presents the CS, CS/5-FU and CS-clay/drug films contact angles and the images of the drops placed on the films.

CS showed an angle value of about 60.5°, close to that reported in the literature [15]. The incorporation of 5-FU in CS increased the contact angle to 65.2°, suggesting that the CS/5-FU film became more hydrophobic. This behavior is likely due to the higher degree of crystallinity, as verified by XRD. As the concentration of MMT increased, the

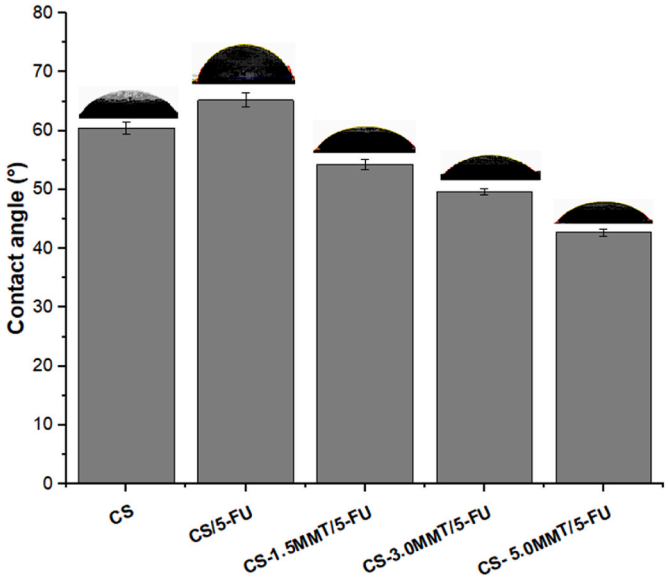


**Fig. 3.** Contact angles of CS, CS/5-FU and CS-MMT/5-FU films.

CS-MMT/5-FU nanocomposite films became more hydrophilic. The most hydrophilic material was the CS-5.0MMT/5-FU film (42.7°), which indicated that the MMT clay increased the interaction with liquid due to its hydrophilic nature [66].

According to the chemical analysis, the CS-5.0MMT/5-FU nanocomposite film showed an amorphous structure, incorporation of 5-FU between the MMT lamellae, homogeneous dispersion of 5-FU in the films, and a highly hydrophilic surface. Due to these properties, the CS-5.0MMT/5-FU nanocomposite film was selected for further analysis.

### 3.3. Swelling degree and in vitro drug release of nanocomposite films

Swelling is one of the most important properties of bionanocomposite films because it controls the release rate of the encapsulated drug and is an indicator of the ease and speed of liquid penetration into the films as well as drug diffusion from the films [49]. Fig. 4 shows the swelling degree as a function of time for the CS, CS/5-FU and

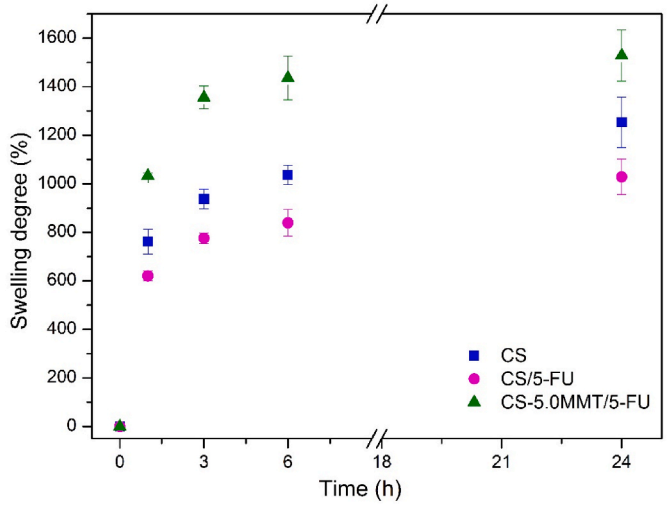


**Fig. 4.** Swelling degree of CS, CS/5-F and CS-5.0MMT/5-FU films vs. time.

CS-5.0MMT/5-FU films evaluated at PBS (pH = 7.2).

All films showed a high degree of swelling with rapid swelling kinetics at 1 h. Over 3–6 h, the curve goes through a transition where the swelling gradually increases to reach a plateau level after 24 h (saturation level). A greater degree of swelling was observed for CS as compared to CS/5-FU, showing a greater diffusion capacity for PBS. The CS/5-FU film seems to inhibit the PBS diffusion due to its higher degree of crystallinity and hydrophobicity, thus reducing the swelling ability. This result was consistent with the literature observation [67] that further crystallization minimizes swelling and inhibits liquid diffusion. The CS-5.0MMT/5-FU nanocomposite film showed the highest degree of swelling compared to CS and CS/5-FU, in agreement with the trend observed for the contact angles. This behavior could be attributed to the presence of MMT in this nanocomposite which made the film more hydrophilic and to the intermolecular interactions between water molecules in clay galleries and the ion pair electrons of $–NH_2$ and –OH bonds present in chitosan chains [35]. Similar behavior has been reported in the literature for CS/clay/glycerol-based [68] and CS-PVA/MMT/5-FU [35] nanocomposite films.

Fig. 5 shows the 5-FU release profile of CS/5-FU and CS-5.0MMT/5-FU films. Almost 71% of 5-FU was released from CS/5-FU within 1 h,

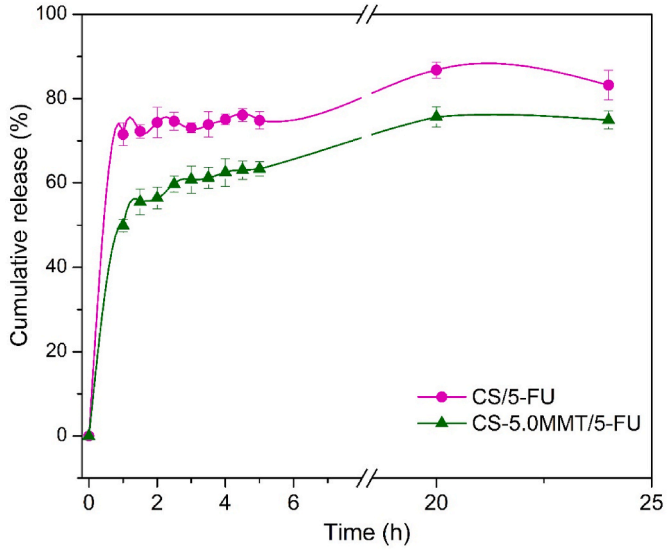


**Fig. 5.** *In vitro* release profile of 5-FU form CS/5-FU and CS-5.0MMT/5-FU films in PBS (pH 7.2 at 37 ± 0.5 °C).

followed by slight variations up to 5 h. The maximum release took place at 20 h (86%), and then a slight reduction to 83% was observed after 24 h. This suggests that the amount of drug in the CS/5-FU film started to decline after 20 h. On the other hand, the film with MMT showed a different behavior. The CS-5.0MMT/5-FU film showed a reduction in the amount of the drug released, releasing about 49% of 5-FU in the first hour followed by a progressive increase up to 20 h, reaching 74% at 24 h. Therefore, incorporating MMT into CS favored a controllable release of 5-FU, especially when 5 wt% of MMT was employed. This reduction in the drug release profile was also observed by other authors after an increase in the amount of clay on the composites and can be explained by the intercalation of 5-FU in silicate layers of the MMT resulting in a suppression of the drug release [34]. Such behavior suggested that the clay dispersion in CS reduced the diffusion rate of 5-FU, thus decreasing the initial release of the drug and prolonging the release profile of 5-FU compared to the CS/5-FU film.

In both formulations, immediately after the contact of the films with the release medium, a larger amount of drug was liberated before the release rate became constant, a typical behavior known as “burst release” [34]. With the addition of MMT the burst step of CS-5.0MMT/5-FU film was less pronounced. This reduction was beneficial because help to control the amount of 5-FU delivered on the first step and reduce the amount delivered in the next steps. This decrease in release rate helps to reduce the toxicity and negative effects of 5-FU [31]. Nevertheless, even with the addition of MMT, the CS-5.0MMT/5-FU film continued to show an “abrupt” 5-FU release. Some authors pointed out that this behavior is negative because it reduces the effective useful life of the drug [34]; however, this behavior can have a positive effect, since the drug reaches the best therapeutic concentration more quickly, making the sustained release profile more effective in preserving of the drug remaining in the body in the best therapeutic concentration ranges [36].

Regarding the possible kinetic profile of 5-FU release from nanocomposite films, other authors pointed out that the rapid initial release occurs mainly due to the dissolution and diffusion of the drug trapped near or on the surface of the film and the second “slower” phase involves the diffusion of the drug. trapped in the internal part of the polymer matrix [34,69]. Thus, the release of the 5-FU present in the nanocomposite film was possibly guided by a dissolution and diffusion step in the first hours followed by a final diffusion step.

As a result, the CS-5.0MMT/5-FU nanocomposite film offers promise as a more manageable method of drug delivery since the release profile can be controlled according to the amount of clay added to the film and the fact that it keeps the drug concentration within the therapeutic range for long periods [36]. This is key to improved treatment effectiveness, lowering harmful levels and limiting side effects [58].

### 3.4. Microbiological activity of 5-FU, CS/5-FU and CS-5.0MMT/5-FU

One of the essential features required in a dressing is the control of bacterial growth in wounds [70]. Some cancer-related lesions, such as Squamous Cell Carcinoma and Keratoacanthoma, result in skin wounds, creating a potential focus for infection [71,72]. Therefore, it is crucial that dressings designed for skin cancer treatment also demonstrate the ability to control microbial growth. Thus, the antimicrobial activity of the 5-FU solution (125 mg $L^{-1}$) and the CS/5-FU and CS-5.0MMT/5-FU films were tested against *S. aureus* (ATCC 13656), *E. coli* (ATCC 25422), and *C. albicans* (ATCC 76645) using the disk diffusion method, and the relevant results can be observed in Fig. 6 and Table 3.

In the agar disk diffusion method, the bactericidal/antifungal activity of the material is a function of the size of the halo opening around the sample. In other words, the larger the halo, the greater the bactericidal/antifungal activity. According to the results, all samples showed strong microbiological activity against *S. aureus*, *E. coli*, and *C. albicans*. The CS-5.0MMT/5-FU film obtained the largest inhibition halos with 46.33 and 37.33 mm for *S. aureus* and *E. coli* strains, respectively, and

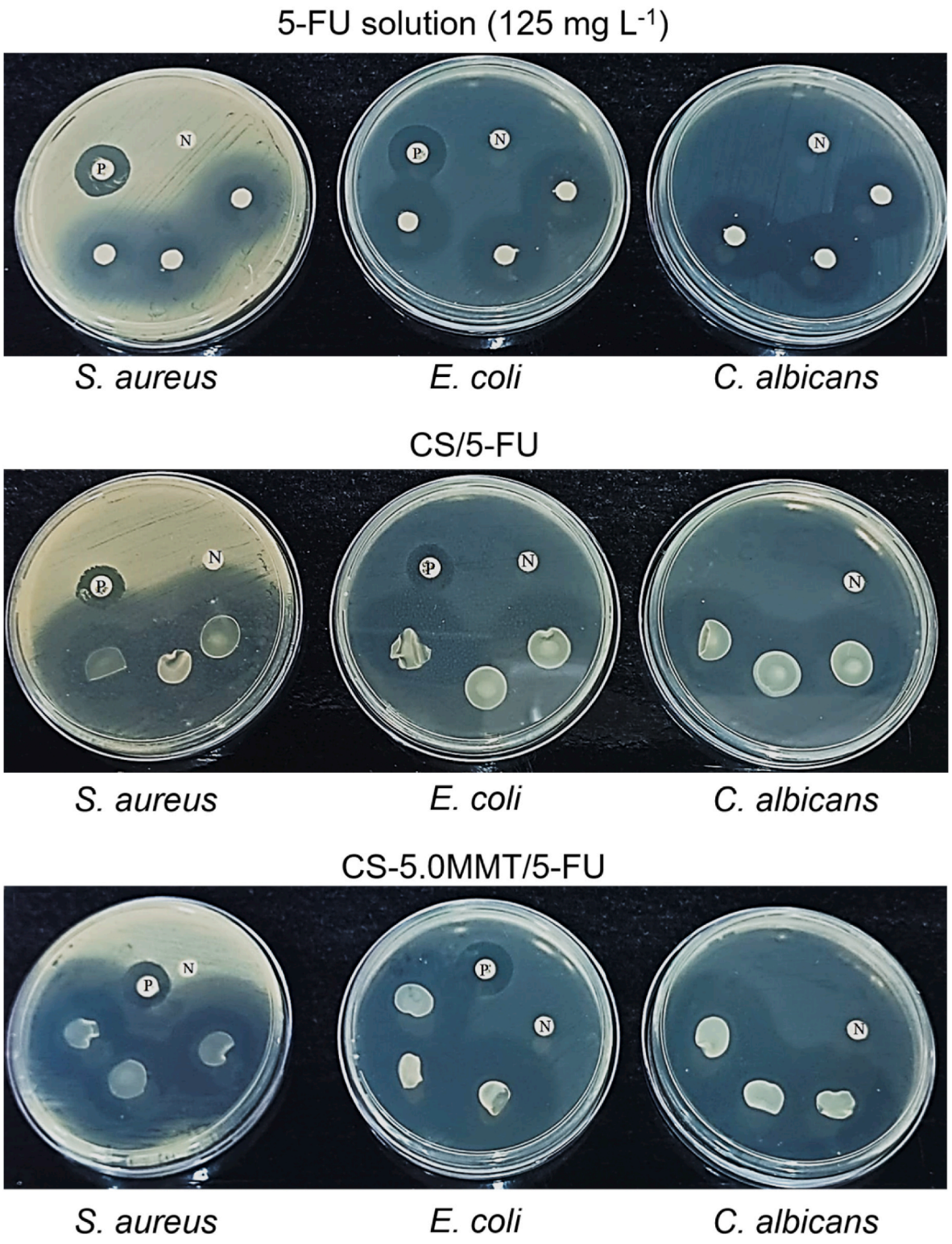


**Fig. 6.** The antibacterial/antifungal activity of 5-FU solution, CS/5-FU, and CS-5.0MMT/5-FU films against *S. aureus*, *E. coli*, and *C. albicans* evaluated using the disk-diffusion method. The analyses were performed in triplicate for each sample.

the CS/5-FU film with 35.67 mm for the *C. albicans* strain. On the other hand, the 5-FU solution had the smallest inhibition halos. However, together with the films, it had superior activity to the positive control - vancomycin, an antibiotic used to combat bacterial infections.

The drug 5-FU is well known for its use in cancer treatment and also exhibits bactericidal activity. Its molecular structure contains fluorine and oxo groups that play positive roles in its bioactivity [65]. These groups allow 5-FU to bind to DNA, interrupting its synthesis. Studies have shown that 5-FU has bactericidal activity against a wide range of Gram-positive and Gram-negative microorganisms, including *S. aureus* and *E. coli*, at concentrations below 100 μg $mL^{-1}$ [66]. Other authors have explored the bactericidal activity of 5-FU by using it in the synthesis of hybrid compounds. In their results, the authors suggested hydrogen bonding between the oxygen and fluorine atoms in the

**Table 3**
Antimicrobial activity 5-FU solution, CS/5-FU and CS-5.0MMT/5-FU films against *S. aureus*, *E. coli*, and *C. albicans* strains in MHB culture media.

| Samples | Inhibition zone (mm)* | | |
|---|---|---|---|
| | *S. aureus* (ATCC 13656) | *E. coli* (ATCC 25422) | *C. albicans* (ATCC 76645) |
| Negative control | 0 | 0 | 0 |
| Positive control | 15.67 ± 1.15 | 18 | – |
| 5-FU solution | 25.33 ± 0.58 | 26.00 ± 1.73 | 23.33 ± 0.58 |
| CS/5-FU | 45.33 ± 2.52 | 36.00 ± 1.00 | 35.67 ± 0.58 |
| CS-5.0MMT/5-FU | 46.33 ± 0.58 | 37.33 ± 0.58 | 34.33 ± 2.08 |

structure of 5-FU and DNA. This interaction between the hybrids and DNA provided good or even superior antimicrobial activity compared to that of positive controls, chloramphenicol, norfloxacin, and fluconazole, against various bacterial and fungal strains, including *S. aureus*, *E. coli*, and *C. albicans* [65].

The CS films loaded with 5-FU exhibited higher bactericidal activity than the tested 5-FU solution. This effect can be explained by the bactericidal activity also exhibited by CS [5–7]. Similar results were observed by Reddy et al. [35], who observed bactericidal activity of their CS/PVA/$Na^+$MMT nanocomposite films from the combination of CS, MMT, and 5-FU. With the addition of clay, the bactericidal activity of the CS-clay/drug film was slightly improved. This is due to the more gradual release of 5-FU, which made it possible to maintain its release for a longer period within the therapeutic range.

Therefore, these results indicate a synergistic bactericidal action of 5-FU with CS, which was optimized by the incorporation of MMT that modulated the delivery of 5-FU, keeping it within the therapeutic range [54], resulting in a better bactericidal activity of the CS-5.0MMT/5-FU nanocomposite. Thus, the CS-5.0MMT/5-FU film was found to be efficient in controlling the growth of microorganisms commonly found in external skin lesions.

### 3.5. Cytotoxicity test in vitro – diffusion agar method

Table 4 and Fig. 7 show the results and the evolution of the cytotoxicity of the CS, CS/5-FU and CS-5.0MMT/5-FU films towards L929 fibroblastic cells. After 24 h of incubation, the halo size around the samples was measured using the scoring criteria (Table 2). The growth, positive and negative controls were utilized to validate the cytotoxicity assay efficiency. The CS and CS/5-FU films performed similarly, with halo values in the range of 0.138 and 0.238 cm, which were much lower than the positive control. The halo increase observed in the CS/5-FU film can be attributed to the cytotoxic effect of 5-FU on the cells. However, this effect was not significant enough to alter the degree of cytotoxicity of the CS/5-FU sample. Thus, even though the CS and CS/5-FU films induced cell death or harm to the cell population according to ISO-10993-5 classification standards, their cytotoxicity fell into the low reactivity category, with a level of 2 (zone limited to the area under specimen), corresponding to a low level of reactivity.

As a result of the presence of clay, no cell death was seen with the CS-5.0MMT/5-FU nanocomposite film; however, the presence of some malformed or degenerated cells was observed under the specimen, which according to the ISO-10993-5 indicated light cytotoxicity (grade 1). These findings are consistent with the 5-FU release profile, which showed that the clay incorporation delayed its release and, consequently, reduced the cytotoxic impact caused by 5-FU on the cells. Similar results were observed by Kevadiya et al. [32] who compared the cell viability of A549 cells to 5-FU, 5-FU-MMT and CS-MMT/5-FU nanocomposites and observed that the CS-MMT/5-FU composite showed the highest cell viability at all times between 0 and 72 h of incubation, noting a reduction in the cytoxicity of the samples with MMT. Thus, the toxicity of 5-FU was reduced as a result of better control over its release due to higher encapsulation by the clay. These findings are also consistent with earlier studies published in the literature, in which the addition of MMT contributed to a reduction in drug release [32,34,35] and a reduction of 5-FU side effects in healthy cells [31,32], without affecting 5-FU antitumor effectiveness [32,33]. Furthermore, the CS-5.0MMT/5-FU nanocomposite was less hazardous than the CS film due to MMT's neutralization of reactive acid groups present in the CS, as previously described [73]. Thus, the CS-5.0MMT/5-FU demonstrated to be biocompatible *in vitro*, with no adverse effects and shows promise for usage in controlled release of 5-FU.

**Table 4**
Cytotoxicity assessment (L929 cells) using the agar test.

| Samples | Average plate readings (cm) | Degree of cytotoxicity |
|---|---|---|
| Negative control | 0 | 0 |
| Positive control | 0.650 | 3 |
| CS | 0.138 | 2 |
| CS/5-FU | 0.238 | 2 |
| CS-5.0MMT/5-FU | 0 | 0 |

### 3.6. Limitations of the present study and future works

While our investigation has provided insights into the potential of the CS/MMT/5-FU nanocomposite film as a biomaterial for the treatment of skin malignancies, it is important to discuss about certain limitations and identify avenues for future research. The following discusses the constraints of the present study and outlines potential directions for future work:

- The main goal of this study was to study the CS/MMT/5-FU nanocomposite film's physicochemical properties, drug release profile, cytotoxicity, and microbiological properties. However, a direct investigation into the antitumor efficacy of skin cancer was not conducted. In-depth cytotoxicity or pharmacodynamic studies should be included in future research projects to confirm that the nanocomposite film has the potential to treat tumors.
- While our study included an agar diffusion assay to assess cytotoxicity, we acknowledge that additional MTT or CCK-8 experiments are needed for a more comprehensive evaluation of biosafety. To address this limitation, future works should prioritize the inclusion of MTT or CCK-8 experiments to further substantiate the biosafety of the CS/MMT/5-FU nanocomposite film.
- This study demonstrated the potential of the nanocomposite film to slow down and extend the release rate of 5-FU. However, the investigation primarily focused on controlled release capabilities within a specific timeframe. Future research could delve deeper into optimizing and extending the release duration, considering factors such as varying concentrations, additional drug loading strategies, and more intricate release profiles.
- To bridge the gap between laboratory findings and clinical application, future research should consider conducting in vivo studies to validate the efficacy and safety of the CS/MMT/5-FU nanocomposite film. This would provide a more comprehensive understanding of its potential as a therapeutic intervention for skin cancer.

Finally, while the present study lays a foundation for developing the CS/MMT/5-FU nanocomposite film, addressing these limitations through future research will contribute to a more thorough and robust evaluation of its biomedical applications.

## 4. Conclusions

Using solvent evaporation, we successfully synthesized a CS/MMT nanocomposite film to be used as a drug delivery system for the

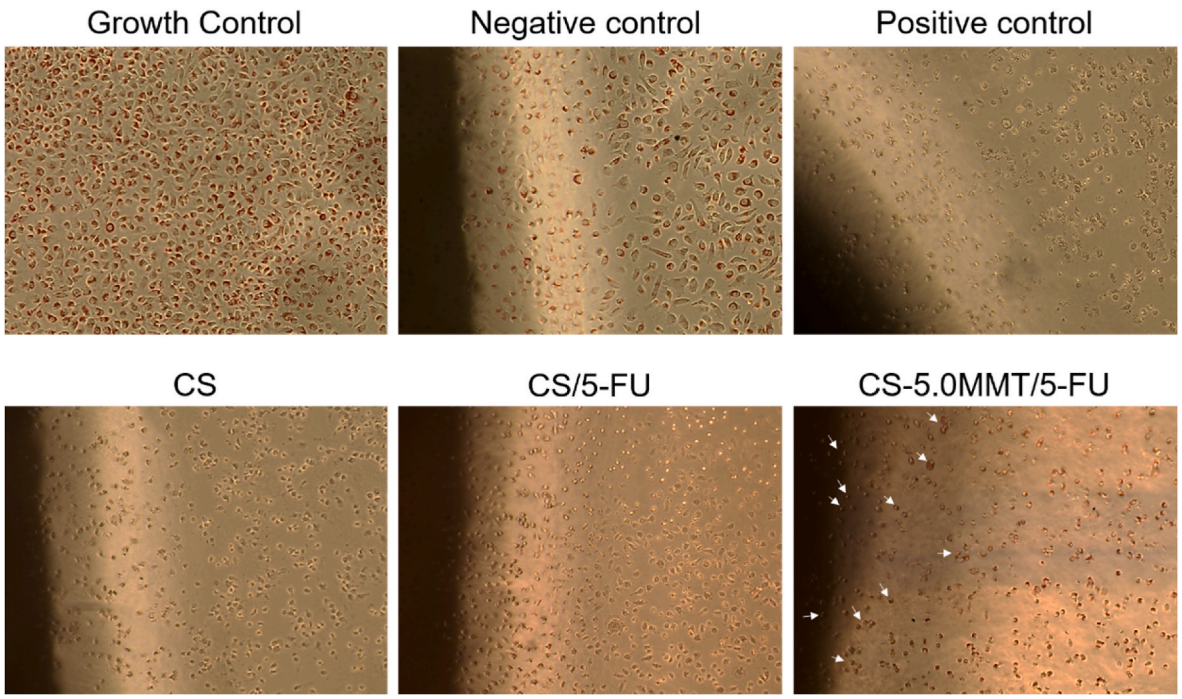


**Fig. 7.** Optical microscopy images of cytotoxicity tests using L929 fibroblastic cells. The arrows indicate the presence of live cells around and below the CS-5.0MMT/5-FU nanocomposite film.

controlled release of the anticancer drug 5-FU. The incorporation of MMT into the chitosan matrix resulted in an intercalated nanocomposite, where the drug 5-FU established molecular-level interactions with chitosan and positioned itself between the MMT layers. XRD and FTIR spectra confirmed the successful encapsulation of 5-FU in the CS matrix and revealed the interactions between chitosan and 5-FU, along with the increased concentration of clay. This increase in clay concentration also modified the chemical properties of the nanocomposite films, reducing the contact angle and increasing the swelling capability.

The CS-clay/drug nanocomposite film demonstrated a significant reduction in the drug release profile when compared to the chitosan film with 5-FU alone. The inclusion of MMT in the CS matrix slowed down the release of 5-FU by confining it in the clay layers, contributing to the improved microbiological activity of the CS-clay/drug nanocomposite film against *S. aureus* and *E. coli*. Furthermore, the toxicity of 5-FU was minimized, as demonstrated by the cytotoxicity assay, which indicated that the nanocomposite film with a higher concentration of MMT was non-toxic to L929 fibroblast cells.

Given that the nanocomposite has the potential to slow down and extend the release rate of 5-FU in a safe and targeted manner with appropriate release capabilities, the CS-clay/drug nanocomposite film is a promising alternative biomaterial for the treatment of skin cancer and other external malignancies.

## Declaration of competing interest

The authors declare that they have no known competing financial interests or personal relationships that could have appeared to influence the work reported in this paper.

## Acknowledgments

The present work was carried out with the support of the Coordination for the Improvement of Higher Education Personnel - Brazil (CAPES).

## References

[1] R. Langer, Biomaterials in drug delivery and tissue Engineering: one laboratory's experience, Acc. Chem. Res. 33 (2000) 94–101. https://pubs.acs.org/doi/10.1021/ar9800993.
[2] T.L. Cao, S.-Y. Yang, K.B. Song, Development of burdock root inulin/chitosan blend films containing oregano and thyme essential oils, Int. J. Mol. Sci. 19 (2018) 131, https://doi.org/10.3390/ijms19010131.
[3] L. Sun, J. Sun, L. Chen, P. Niu, X. Yang, Y. Guo, Preparation and characterization of chitosan film incorporated with thinned young apple polyphenols as an active packaging material, Carbohydr. Polym. 163 (2017) 81–91, https://doi.org/10.1016/j.carbpol.2017.01.016.
[4] D.M.S. Wanderley, D.F. Melo, L.M. Silva, J.W.L. Souza, H.V. Pina, D.B. Lima, S.K. S. Amoah, S.M.P. Borges, M.V.L. Fook, R.O. Moura, R.S.C. Lima, B. Damasceno, Biocompatibility and mechanical properties evaluation of chitosan films containing an N-acylhydrazonic derivative, Eur. J. Pharmaceut. Sci. 155 (2020) 105547, https://doi.org/10.1016/j.ejps.2020.105547.
[5] C. Choi, J.-P. Nam, J.-W. Nah, Application of chitosan and chitosan derivatives as biomaterials, J. Ind. Eng. Chem. 33 (2016) 1–10, https://doi.org/10.1016/j.jiec.2015.10.028.
[6] M.N.V. Ravi Kumar, A review of chitin and chitosan applications, React. Funct. Polym. 46 (2000) 1–27, https://doi.org/10.1016/S1381-5148(00)00038-9.
[7] O.M. Dragostin, S.K. Samal, M. Dash, F. Lupascu, A. Pânzariu, C. Tuchilus, N. Ghetu, M. Danciu, P. Dubruel, D. Pieptu, C. Vasile, R. Tatia, L. Profire, New antimicrobial chitosan derivatives for wound dressing applications, Carbohydr. Polym. 141 (2016) 28–40, https://doi.org/10.1016/j.carbpol.2015.12.078.
[8] M. Dash, F. Chiellini, R.M. Ottenbrite, E. Chiellini, Chitosan—a versatile semi-synthetic polymer in biomedical applications, Prog. Polym. Sci. 36 (2011) 981–1014, https://doi.org/10.1016/j.progpolymsci.2011.02.001.
[9] D.K. Singh, A.R. Ray, Biomedical applications of chitin, chitosan, and their derivatives, J. Macromol. Sci., Part C 40 (2000) 69–83, https://doi.org/10.1081/MC-100100579.
[10] H.D.C. Barbosa, B.F.F.d. Santos, A.A. Tavares, R.C. Barbosa, M.V.L. Fook, E. L. Canedo, S.M.d.L. Silva, Inexpensive Apparatus for fabricating microspheres for 5-fluorouracil controlled release systems, Int. J. Chem. Eng. 2018 (2018) 2340249, https://doi.org/10.1155/2018/2340249.
[11] M. Rahbar, A. Morsali, M.R. Bozorgmehr, S.A. Beyramabadi, Quantum chemical studies of chitosan nanoparticles as effective drug delivery systems for 5-fluorouracil anticancer drug, J. Mol. Liq. 302 (2020) 112495, https://doi.org/10.1016/j.molliq.2020.112495.
[12] V. Campani, E. Pagnozzi, I. Mataro, L. Mayol, A. Perna, F. D'Urso, A. Carillo, M. Cammarota, M.C. Maiuri, G. De Rosa, Chitosan gel to treat pressure ulcers: a clinical pilot study, Pharm. Times 10 (2018), https://doi.org/10.3390/pharmaceutics10010015.
[13] H.N. da Silva, M.C. da Silva, F.S.F. Dos Santos, J.A.C. da Silva Júnior, R.C. Barbosa, M.V.L. Fook, Chitosan woven meshes: influence of threads configuration on mechanical, morphological, and physiological properties, Polym 13 (2020), https://doi.org/10.3390/polym13010047.

[14] A.K. Mahanta, D.K. Patel, P. Maiti, Nanohybrid scaffold of chitosan and functionalized graphene oxide for controlled drug delivery and bone regeneration, ACS Biomater. Sci. Eng. 5 (2019) 5139–5149. https://pubs.acs.org/doi/10.1021/acsbiomaterials.9b00829.
[15] H.Y.C. Eulálio, M. Vieira, T.B. Fideles, H. Tomás, S.M.L. Silva, C.A. Peniche, M.V. L. Fook, Physicochemical properties and cell viability of shrimp chitosan films as affected by film casting solvents. I-potential use as wound dressing, Materials 13 (2020), https://doi.org/10.3390/ma13215005.
[16] I.A. Sogias, V.V. Khutoryanskiy, A.C. Williams, Exploring the factors affecting the solubility of chitosan in water, Macromol. Chem. Phys. 211 (2010) 426–433, https://doi.org/10.1002/macp.200900385.
[17] M.S.A. Darwish, M.H. Mostafa, L.M. Al-Harbi, Polymeric nanocomposites for environmental and industrial applications, Int. J. Mol. Sci. 23 (2022), https://doi.org/10.3390/ijms23031023.
[18] B. Almuallim, W.S.W. Harun, I.J. Al Rikabi, H.A. Mohammed, Thermally conductive polymer nanocomposites for filament-based additive manufacturing, J. Mater. Sci. 57 (2022) 3993–4019, https://doi.org/10.1007/s10853-021-06820-2.
[19] F. Altunkaynak, M. Okur, N. Saracoglu, Controlled release of paroxetine from chitosan/montmorillonite composite films, J. Drug Deliv. Sci. Technol. 68 (2022) 103099, https://doi.org/10.1016/j.jddst.2022.103099.
[20] S. Jayrajsinh, G. Shankar, Y.K. Agrawal, L. Bakre, Montmorillonite nanoclay as a multifaceted drug-delivery carrier: a review, J. Drug Deliv. Sci. Technol. 39 (2017) 200–209, https://doi.org/10.1016/j.jddst.2017.03.023.
[21] M. Wiles, H. Huebner, E. Afriyie-Gyawu, R. Taylor, G. Bratton, T. Phillips, Toxicological evaluation and metal bioavailability in pregnant rats following exposure to clay minerals in the diet, J. Toxicol. Environ. 67 (2004) 863–874, https://doi.org/10.1080/15287390490425777.
[22] G. Thakur, A. Singh, I. Singh, Chitosan-montmorillonite polymer composites: formulation and evaluation of sustained release tablets of aceclofenac, Sci. Pharm. 84 (2015) 603–617, https://doi.org/10.3390/scipharm84040603.
[23] I. Salcedo, C. Aguzzi, G. Sandri, M.C. Bonferoni, M. Mori, P. Cerezo, R. Sánchez, C. Viseras, C. Caramella, In vitro biocompatibility and mucoadhesion of montmorillonite chitosan nanocomposite: a new drug delivery, Appl. Clay Sci. 55 (2012) 131–137, https://doi.org/10.1016/j.clay.2011.11.006.
[24] E.P. Rebitski, G.P. Souza, S.A.A. Santana, S.B.C. Pergher, A.C.S. Alcântara, Bionanocomposites based on cationic and anionic layered clays as controlled release devices of amoxicillin, Appl. Clay Sci. 173 (2019) 35–45, https://doi.org/10.1016/j.clay.2019.02.024.
[25] X. Wang, Y. Du, J. Luo, Biopolymer/montmorillonite nanocomposite: preparation, drug-controlled release property and cytotoxicity, Nanotechnology 19 (2008) 065707, https://doi.org/10.1088/0957-4484/19/6/065707.
[26] I. Salcedo, G. Sandri, C. Aguzzi, C. Bonferoni, P. Cerezo, R. Sánchez-Espejo, C. Viseras, Intestinal permeability of oxytetracycline from chitosan-montmorillonite nanocomposites, Colloids Surf., B 117 (2014) 441–448, https://doi.org/10.1016/j.colsurfb.2013.11.009.
[27] D.B. Longley, D.P. Harkin, P.G. Johnston, 5-Fluorouracil: mechanisms of action and clinical strategies, Nat. Rev. Cancer 3 (2003) 330–338, https://doi.org/10.1038/nrc1074.
[28] S. Vodenkova, T. Buchler, K. Cervena, V. Veskrnova, P. Vodicka, V. Vymetalkova, 5-fluorouracil and other fluoropyrimidines in colorectal cancer: past, present and future, Pharmacol. Ther. 206 (2020) 107447, https://doi.org/10.1016/j.pharmthera.2019.107447.
[29] C. Sethy, C.N. Kundu, 5-Fluorouracil (5-FU) resistance and the new strategy to enhance the sensitivity against cancer: implication of DNA repair inhibition, Biomed. Pharmacother. 137 (2021) 111285, https://doi.org/10.1016/j.biopha.2021.111285.
[30] K. Hodroj, D. Barthelemy, J.C. Lega, G. Grenet, M.C. Gagnieu, T. Walter, J. Guitton, L. Payen-Gay, Issues and limitations of available biomarkers for fluoropyrimidine-based chemotherapy toxicity, a narrative review of the literature, ESMO Open 6 (2021) 100125, https://doi.org/10.1016/j.esmoop.2021.100125.
[31] S. Handali, E. Moghimipour, M. Rezaei, S. Saremy, F.A. Dorkoosh, Co-delivery of 5-fluorouracil and oxaliplatin in novel poly(3-hydroxybutyrate-co-3-hydroxyvalerate acid)/poly(lactic-co-glycolic acid) nanoparticles for colon cancer therapy, Int. J. Biol. Macromol. 124 (2019) 1299–1311, https://doi.org/10.1016/j.ijbiomac.2018.09.119.
[32] B.D. Kevadiya, T.A. Patel, D.D. Jhala, R.P. Thumbar, H. Brahmbhatt, M.P. Pandya, S. Rajkumar, P.K. Jena, G.V. Joshi, P.K. Gadhia, C.B. Tripathi, H.C. Bajaj, Layered inorganic nanocomposites: a promising carrier for 5-fluorouracil (5-FU), Eur. J. Pharm. Biopharm. 81 (2012) 91–101, https://doi.org/10.1016/j.ejpb.2012.01.004.
[33] R. Surya, M.D. Mullassery, N.B. Fernandez, D. Thomas, Alginate-bentonite composite decorated by chitosan-folate conjugate for the oral delivery of 5-Fluorouracil, Lett. Org. Chem. 13 (2023) 461–474, https://doi.org/10.1080/22297928.2023.2263018.
[34] F. Farshi Azhar, A. Olad, A study on sustained release formulations for oral delivery of 5-fluorouracil based on alginate–chitosan/montmorillonite nanocomposite systems, Appl. Clay Sci. 101 (2014) 288–296, https://doi.org/10.1016/j.clay.2014.09.004.
[35] A.B. Reddy, B. Manjula, T. Jayaramudu, E.R. Sadiku, P. Anand Babu, S. Periyar Selvam, 5-Fluorouracil loaded chitosan–PVA/Na+MMT nanocomposite films for drug release and antimicrobial activity, Nano-Micro Lett. 8 (2016) 260–269, https://doi.org/10.1007/s40820-016-0086-4.
[36] M.R. Abukhadra, N.M. Refay, A.M. El-Sherbeeny, A.M. Mostafa, M.A. Elmeligy, Facile synthesis of bentonite/biopolymer composites as low-cost carriers for 5-fluorouracil drug; equilibrium studies and pharmacokinetic behavior, Int. J. Biol. Macromol. 141 (2019) 721–731, https://doi.org/10.1016/j.ijbiomac.2019.09.057.
[37] I. Sivanesan, J. Gopal, M. Muthu, J. Shin, S. Mari, J. Oh, Green synthesized chitosan/chitosan nanoforms/nanocomposites for drug delivery applications, Polym 13 (2021) 2256, https://doi.org/10.3390/polym13142256.
[38] B.J. Rider, in: S.J. Enna, D.B. Bylund (Eds.), xPharm: the Comprehensive Pharmacology Reference, Elsevier, New York, 2007, pp. 1–5.
[39] S. Goindi, B. Dhatt, A. Kaur, Ethosomes-based topical delivery system of antihistaminic drug for treatment of skin allergies, J. Microencapsul. 31 (2014) 716–724, https://doi.org/10.3109/02652048.2014.918667.
[40] E. Proksch, pH in nature, humans and skin, J. Dermatol. 45 (2018) 1044–1052, https://doi.org/10.1111/1346-8138.14489.
[41] L. Kaewsichan, D. Riyapan, P. Prommajan, J. Kaewsrichan, Effects of sintering temperatures on micro-morphology, mechanical properties, and bioactivity of bone scaffolds containing calcium silicate, Sci. Asia 37 (2011) 240–246, https://doi.org/10.1038/s41598-017-00905-2.
[42] J.Z. Kubicek-Sutherland, N.S. Makarov, Z.R. Stromberg, K.D. Lenz, C. Castañeda, A. N. Mercer, H. Mukundan, H. McDaniel, K. Ramasamy, Exploring the biocompatibility of near-IR CuInSexS2–x/ZnS quantum dots for deep-tissue bioimaging, ACS Appl. Bio Mater. 3 (2020) 8567–8574, https://doi.org/10.1021/acsabm.0c00939.
[43] U.E. Illangakoon, D.-G. Yu, B.S. Ahmad, N.P. Chatterton, G.R. Williams, 5-Fluorouracil loaded Eudragit fibers prepared by electrospinning, Int. J. Pharm. 495 (2015) 895–902, https://doi.org/10.1016/j.ijpharm.2015.09.044.
[44] K.L. Nair, S. Jagadeeshan, S.A. Nair, G.S. Kumar, Biological evaluation of 5-fluorouracil nanoparticles for cancer chemotherapy and its dependence on the carrier, PLGA, Int. J. Nanomed. 6 (2011) 1685–1697, https://doi.org/10.2147/IJN.S20165.
[45] P. Li, Y. Wang, Z. Peng, F. She, L. Kong, Development of chitosan nanoparticles as drug delivery systems for 5-fluorouracil and leucovorin blends, Carbohydr. Polym. 85 (2011) 698–704, https://doi.org/10.1016/j.carbpol.2011.03.045.
[46] B.F.F. dos Santos, M.A. Maciel, A.A. Tavares, C.Q.B. de Araújo Fernandes, W.J. B. de Sousa, M.V. Lia Fook, I. Farias Leite, S.M. De Lima Silva, Synthesis and preparation of chitosan/clay microspheres: effect of process parameters and clay type, Materials 11 (2018) 2523, https://doi.org/10.3390/ma11122523.
[47] P. Borralleras, I. Segura, M.A.G. Aranda, A. Aguado, Influence of experimental procedure on d-spacing measurement by XRD of montmorillonite clay pastes containing PCE-based superplasticizer, Cement Concr. Res. 116 (2019) 266–272, https://doi.org/10.1016/j.cemconres.2018.11.015.
[48] M. Pospíšil, P. Čapková, D. Měřínská, Z. Maláč, J. Šimoník, Structure analysis of montmorillonite intercalated with cetylpyridinium and cetyltrimethylammonium: molecular simulations and XRD analysis, J. Colloid Interface Sci. 236 (2001) 127–131, https://doi.org/10.1006/jcis.2000.7360.
[49] C. Tang, N. Chen, Q. Zhang, K. Wang, Q. Fu, X. Zhang, Preparation and properties of chitosan nanocomposites with nanofillers of different dimensions, Polym. Degrad. Stabil. 94 (2009) 124–131, https://doi.org/10.1016/j.polymdegradstab.2008.09.008.
[50] M. Lavorgna, I. Attianese, G.G. Buonocore, A. Conte, M.A. Del Nobile, F. Tescione, E. Amendola, MMT-supported Ag nanoparticles for chitosan nanocomposites: structural properties and antibacterial activity, Carbohydr. Polym. 102 (2014) 385–392, https://doi.org/10.1016/j.carbpol.2013.11.026.
[51] P.C. Srinivasa, M.N. Ramesh, K.R. Kumar, R.N. Tharanathan, Properties of chitosan films prepared under different drying conditions, J. Food Eng. 63 (2004) 79–85, https://doi.org/10.1016/S0260-8774(03)00285-1.
[52] Y. Wan, K.A.M. Creber, B. Peppley, V.T. Bui, Ionic conductivity of chitosan membranes, Polymer 44 (2003) 1057–1065, https://doi.org/10.1016/S0032-3861(02)00881-9.
[53] R.J. Samuels, Solid state characterization of the structure of chitosan films, J. Polym. Sci. B Polym. Phys. 19 (1981) 1081–1105, https://doi.org/10.1002/pol.1981.180190706.
[54] K. Ogawa, Effect of heating an aqueous suspension of chitosan on the crystallinity and polymorphs, Agric. Biol. Chem. 55 (1991) 2375–2379, https://doi.org/10.1080/00021369.1991.10870939.
[55] A. Giannakas, K. Grigoriadi, A. Leontiou, N.-M. Barkoula, A. Ladavos, Preparation, characterization, mechanical and barrier properties investigation of chitosan–clay nanocomposites, Carbohydr. Polym. 108 (2014) 103–111, https://doi.org/10.1016/j.carbpol.2014.03.019.
[56] S.F. Wang, L. Shen, Y.J. Tong, L. Chen, I.Y. Phang, P.Q. Lim, T.X. Liu, Biopolymer chitosan/montmorillonite nanocomposites: preparation and characterization, Polym. Degrad. Stabil. 90 (2005) 123–131, https://doi.org/10.1016/j.polymdegradstab.2005.03.001.
[57] M. Darder, M. Colilla, E. Ruiz-Hitzky, Biopolymer−Clay nanocomposites based on chitosan intercalated in montmorillonite, Chem. Mater. 15 (2003) 3774–3780, https://doi.org/10.1021/cm0343047.
[58] H. Farhadnejad, S.A. Mortazavi, S. Jamshidfar, A. Rakhshani, H. Motasadizadeh, Y. Fatahi, A. Mahdieh, B. Darbasizadeh, Montmorillonite-famotidine/chitosan bio-nanocomposite hydrogels as a mucoadhesive/gastroretentive drug delivery system, Iran. J. Pharm. Res. (IJPR) 21 (2022) e127035, https://doi.org/10.5812/ijpr-127035.
[59] O. Alekseeva, A. Noskov, E. Grishina, L. Ramenskaya, N. Kudryakova, V. Ivanov, A. Agafonov, Structural and thermal properties of montmorillonite/ionic liquid composites, Materials 12 (2019) 2578, https://doi.org/10.3390/ma12162578.
[60] L. Zhao, Y. Hu, D. Xu, K. Cai, Surface functionalization of titanium substrates with chitosan–lauric acid conjugate to enhance osteoblasts functions and inhibit bacteria adhesion, Colloids Surf., B 119 (2014) 115–125, https://doi.org/10.1016/j.colsurfb.2014.05.002.

[61] B.-H. Feng, L.-F. Peng, Synthesis and characterization of carboxymethyl chitosan carrying ricinoleic functions as an emulsifier for azadirachtin, Carbohydr. Polym. 88 (2012) 576–582, https://doi.org/10.1016/j.carbpol.2012.01.002.
[62] V.B. Gavalyan, Synthesis and characterization of new chitosan-based Schiff base compounds, Carbohydr. Polym. 145 (2016) 37–47, https://doi.org/10.1016/j.carbpol.2016.02.076.
[63] E. Robles, E. Villar, M. Alatorre-Meda, M.G. Burboa, M.A. Valdez, P. Taboada, V. Mosquera, Effects of the hydrophobization on chitosan–insulin nanoparticles obtained by an alkylation reaction on chitosan, J. Appl. Polym. Sci. 129 (2013) 822–834, https://doi.org/10.1002/app.38870.
[64] M.H. Abu Elella, A.E. Shalan, M.W. Sabaa, R.R. Mohamed, One-pot green synthesis of antimicrobial chitosan derivative nanocomposites to control foodborne pathogens, RSC Adv. 12 (2022) 1095–1104, https://doi.org/10.1039/D1RA07070C.
[65] W. Yan, W. Chen, U. Muhammad, J. Zhang, H. Zhuang, G. Zhou, Preparation of α-tocopherol-chitosan nanoparticles/chitosan/montmorillonite film and the antioxidant efficiency on sliced dry-cured ham, Food Control 104 (2019) 132–138, https://doi.org/10.1016/j.foodcont.2019.04.026.
[66] Y. Zheng, A. Zaoui, Wetting and nanodroplet contact angle of the clay 2:1 surface: the case of Na-montmorillonite (001), Appl. Surf. Sci. 396 (2017) 717–722, https://doi.org/10.1016/j.apsusc.2016.11.015.
[67] X. Qu, A. Wirsén, A.C. Albertsson, Novel pH-sensitive chitosan hydrogels: swelling behavior and states of water, Polymer 41 (2000) 4589–4598, https://doi.org/10.1016/S0032-3861(99)00685-0.
[68] I. Abdurrahim Kusmono, Water sorption, antimicrobial activity, and thermal and mechanical properties of chitosan/clay/glycerol nanocomposite films, Heliyon 5 (2019) e02342, https://doi.org/10.1016/j.heliyon.2019.e02342.
[69] M. Guyot, F. Fawaz, Design and in vitro evaluation of adhesive matrix for transdermal delivery of propranolol, Int. J. Pharm. 204 (2000) 171–182, https://doi.org/10.1016/S0378-5173(00)00494-4.
[70] P. Deng, J. Chen, L. Yao, P. Zhang, J. Zhou, Thymine-modified chitosan with broad-spectrum antimicrobial activities for wound healing, Carbohydr. Polym. 257 (2021) 117630, https://doi.org/10.1016/j.carbpol.2021.117630.
[71] C. Niu, Y. Liu, J. Wang, Y. Liu, S. Zhang, Y. Zhang, L. Zhang, D. Zhao, F. Liu, L. Chao, X. Wang, C. Zhang, G. Song, Z. Zhang, Y. Li, Z. Yan, Y. Wen, Y. Ge, Z. Zang, W. Feng, H. Zhang, L. Tao, R. Nakyeyune, Y. Shen, Y. Shao, X. Guo, T. Miles, A. Yang, F. Liu, G. Wang, Risk factors for esophageal squamous cell carcinoma and its histological precursor lesions in China: a multicenter cross-sectional study, BMC Cancer 21 (2021) 1034, https://doi.org/10.1186/s12885-021-08764-x.
[72] A.M. Vîlcea, L.E. Stoica, C.V. Georgescu, F.C. Popescu, R.N. Ciurea, I.D. Vîlcea, C. S. Mirea, Clinical, histopathological and immunohistochemical study of keratoacanthoma, Rom, J. Morphol. Embryol. 62 (2021) 445–456, https://doi.org/10.47162/RJME.62.2.10.
[73] V. Ambrogi, D. Pietrella, M. Nocchetti, S. Casagrande, V. Moretti, S. De Marco, M. Ricci, Montmorillonite–chitosan–chlorhexidine composite films with antibiofilm activity and improved cytotoxicity for wound dressing, J. Colloid Interface Sci. 491 (2017) 265–272, https://doi.org/10.1016/j.jcis.2016.12.058.